HUNTING DOWN HORIZON-SCALE EFFECTS WITH MULTI-WAVELENGTH SURVEYS

José Fonseca,[1*] Stefano Camera,[2] Mário G. Santos[1,3], Roy Maartens[1,4]
(Dated: July 17, 2015)
Draft version July 17, 2015

ABSTRACT

Next-generation cosmological surveys will probe ever larger volumes of the Universe, including the largest scales, near and beyond the horizon. On these scales, the galaxy power spectrum carries signatures of local primordial non-Gaussianity (PNG) and horizon-scale General Relativistic (GR) effects. But cosmic variance severely limits detection of horizon-scale effects. In order to beat down cosmic variance, we can combine surveys via the multi-tracer technique. This method benefits from large bias differences between two tracers of the underlying dark matter distribution, which suggests a multi-wavelength combination of large volume surveys that are planned on a similar time-scale. We show that the combination of two contemporaneous surveys, a large neutral hydrogen intensity mapping survey in SKA Phase 1 and a Euclid-like photometric survey, will provide unprecedented constraints on PNG as well as detection of the GR effects. We forecast that the error on local PNG will break through the cosmic-variance limit on cosmic microwave background surveys, and achieve $\sigma(f_{NL}) \simeq 1.37 - 0.48$, depending on assumed priors and the final bias and source counts. Moreover it should make the first measurements of GR effects with $\sim 7\%$ accuracy which are more robust to the assumed fiducial model.

1. INTRODUCTION

Upcoming cosmological surveys will start to probe larger and larger volumes of the Universe, opening new windows to study effects on horizon scales (see e.g. Yoo et al. 2012; Alonso et al. 2015b; Camera et al. 2015; Raccanelli et al. 2015). These effects include primordial non-Gaussianity (PNG) and General Relativistic (GR) horizon-scale effects in the observed power spectrum.

PNG is a key discriminator between different classes of inflation models. Local-type PNG (characterised by the parameter f_{NL}) leaves a frozen imprint on horizon-scale power, allowing us to probe the primordial Universe via the cosmic microwave background (CMB) and large scale structure surveys. The Planck constraint (Planck Collaboration et al. 2015), $\sigma(f_{NL}) \simeq 6.5$ (using the large-scale structure convention), is far stronger than those from current galaxy surveys, but is close to the maximum achievable with CMB experiments, which can only rule out inflation models with relatively large PNG.

Local PNG also induces a scale-dependent correction to the bias of any dark matter tracer (Dalal et al. 2008; Matarrese & Verde 2008). This scale dependence can be probed through the 2-point correlation function of the tracer on very large scales, allowing next-generation surveys to significantly improve on the CMB constraints (see e.g. Giannantonio et al. 2012; Camera et al. 2013; Camera et al. 2015c).

Although our focus is PNG, GR horizon-scale effects are unavoidable, as at this level of sensitivity, neglecting them would bias the result. Moreover, they might hint at

something new if GR breaks down on these scales. These GR effects arise via lightcone observations of dark matter tracers such as the number counts of galaxies (Yoo 2010; Challinor & Lewis 2011; Bonvin & Durrer 2011) or maps of intensity (e.g. the integrated 21cm signal from HI galaxies (Hall et al. 2013)). They include Doppler, Sachs-Wolfe, integrated Sachs-Wolfe and time-delay type terms. The lensing contribution to the clustering power, mediated by magnification bias, can also be significant on horizon scales (Alonso et al. 2015b; Montanari & Durrer 2015).

Cosmic variance becomes a serious obstacle to measurements on the horizon scales where the PNG and GR signals are strongest. Forecasts for next-generation surveys show that GR effects will not be detectable using a single tracer and PNG detection is limited to $\sigma(f_{NL}) > 1$ (Alonso et al. 2015b; Raccanelli et al. 2015). This calls for the multi-tracer technique (MT) (Seljak 2009; McDonald & Seljak 2009) to beat down cosmic variance.

MT has been used to explore improvements in the measurement of f_{NL} (see e.g. McDonald & Seljak 2009; Hamaus et al. 2011; Abramo & Leonard 2013; Ferramacho et al. 2014; Yamauchi et al. 2014). In these works, the lensing and GR contributions to clustering power were ignored. While this may have little effect on $\sigma(f_{NL})$, it can significantly bias the best-fit value extracted from the data (Namikawa et al. 2011; Camera et al. 2015b). MT has also been used to forecast detectability of GR effects by Yoo et al. (2012), but neglecting the lensing contribution and the integrated GR effects. Here, we include all lensing and GR effects, without making any flat-sky approximation, in order to produce forecasts of $\sigma(f_{NL})$ and $\sigma(f_{GR})$, for a specifically selected pair of surveys. The parameter f_{GR} corresponds to the inclusion ($f_{GR} = 1$) or omission ($f_{GR} = 0$) of the GR effects.

The MT technique opens a new observational window

* josecarlos.s.fonseca@gmail.com
[1] Physics Department, University of the Western Cape, Cape Town 7535, South Africa
[2] Jodrell Bank Centre for Astrophysics, The University of Manchester, Manchester M13 9PL, UK
[3] SKA South Africa, The Park, Cape Town 7405, South Africa
[4] Institute of Cosmology & Gravitation, University of Portsmouth, Portsmouth PO1 3FX, UK

into probing large scale signatures in the Universe. In fact, it is a game-changer in the way we design surveys to probe these scales, as volume is no longer the ultimate goal and noise reduction becomes a priority again. In addition to the reduction of cosmic variance, MT also cancels the individual systematics of the two experiments and removes foreground residuals in the HI survey, thus bringing another major advantage over a single-tracer approach.

Here we analyse how the combination of two near-term, contemporaneous surveys will be able to push the detection of PNG below the "barrier" of $\sigma(f_{\rm NL}) \sim 1$. These are an HI intensity mapping survey with Phase 1 of the SKA (Square Kilometre Array) (Santos et al. 2015) and a Dark Energy Task Force Stage IV photometric survey, like Euclid (Laureijs et al. 2011). This multi-wavelength synergetic approach should be able to provide the first confirmation of the GR horizon-scale effects in the not so distant future.

2. THE MULTI-TRACER TECHNIQUE

The theoretical observed fluctuations for a given dark matter tracer A can be written in Fourier space and Newtonian gauge in the form:

$$
\Delta^A = \delta \left\{ b_{\rm G}^A + \Delta b^A + f \frac{k_\parallel^2}{k^2} + E(\mathcal{Q}^A - 1) \frac{k_\perp^2}{k^2} \right.
$$
$$
+ \left[F - \mathrm{i} f \left(b_e^A - 2\mathcal{Q}^A + \frac{2\mathcal{Q}^A}{\mathcal{H}\chi} \right) \frac{k_\parallel}{k} \right] \frac{\mathcal{H}}{k}
$$
$$
\left. + \left[G + f b_e^A + I \mathcal{Q}^A + J \left(b_e^A - 2\mathcal{Q}^A + \frac{2\mathcal{Q}^A}{\mathcal{H}\chi} \right) \right] \frac{\mathcal{H}^2}{k^2} \right\}, \quad (1)
$$

where $\mathbf{k} = (\mathbf{k}_\perp, k_\parallel)$ and $\mathcal{H}$ is the conformal Hubble parameter. The first line contains the RSD and lensing terms, while the next 2 lines constitute the horizon-scale GR terms. The density contrast δ is in the comoving-synchronous gauge in order to define the bias consistently on large scales, and f is its growth rate. The correction to the Gaussian bias $b_{\rm G}$ due to local PNG is given by $\Delta b(k,z) = 3 f_{\rm NL} [b_{\rm G}(z) - 1] \Omega_m H_0^2 \delta_c / [D(z) T(k) k^2]$. Here, $\delta_c \simeq 1.69$ is the critical matter density contrast for spherical collapse, $T(k)$ is the transfer function (normalised to 1 on large scales) and $D(z)$ is the growth factor (normalised to 1 at $z = 0$). The evolution bias is $b_e^A(z) = -\partial \ln[(1 + z)^{-3} n^A(z)] / \partial \ln(1 + z)$ and $\mathcal{Q}^A$ is the magnification bias, which will be discussed later. The background functions E, F, G, I and J are tracer-independent.

We see that PNG grows as k^{-2}, while the GR terms grow as $\mathcal{H}/k$ or $\mathcal{H}^2/k^2$. It is mainly this difference in the scale dependence, together with the amplitude of the different terms, that allows the GR corrections to be distinguishable from the PNG effect. More importantly, the uncertainties due to cosmic variance come from the δ (dark matter) term, since it is a single realisation of the underlying probability distribution. The MT technique relies on the fact that this term is common to both tracers, so that a measurement of the ratio of different Δ's will be independent of this cosmic variance.

To test the MT constraints, the estimator we use is the sky map itself, in the form of the $a_{\ell m}$. Assuming that the distribution of the $a_{\ell m}$ are Gaussian, all

the information will be encoded in the 2-point correlation function or the angular power spectrum, where $\langle a_{\ell m} a_{\ell' m'}^* \rangle = \delta_{\ell \ell'} \delta_{m m'} C_\ell$. Using a Gaussian likelihood for the $a_{\ell m}$, the corresponding Fisher matrix will then be enough to account for the MT effects. The angular power spectrum between two tracers, A and B, is then given by (Challinor & Lewis 2011; Bonvin & Durrer 2011; Hall et al. 2013)

$$
C_\ell \left(z_i^A, z_j^B \right) = 4\pi \int \mathrm{d} \ln k \, \Delta_\ell^A (z_i, k) \, \Delta_\ell^B (z_j, k) \, \mathcal{P}_\zeta (k).
$$
$$(2)$$

Here, z_i are the centres of the redshift bins between which we correlate the signal and $\mathcal{P}_\zeta$ is the dimensionless power spectrum of the primordial curvature perturbation. The measurable transfer function in the bin is

$$
\Delta_\ell^A (z_i, k) = \int \mathrm{d} z \, n^A(z) W(z_i, z) \Delta_\ell^A(z, k), \quad (3)
$$

where $n^A(z)$ is the selection function of tracer A, i.e. the redshift distribution function of observed sources for tracer A. The theoretical transfer function is $\Delta_\ell^A(z, k)$, while $W(z_i, z)$ is the window function centred on z_i, namely the probability distribution function of a source to be inside the ith bin. The product of the selection function and the window function is the effective redshift distribution function of the sources inside the bin, normalised so that $\int \mathrm{d} z \, n^A(z) W(z_i, z) = 1$ for all z_i's.

3. MULTI-WAVELENGTH SURVEYS

In order to optimally exploit the MT method, we look for two surveys with significant difference in bias. A particularly interesting option would be an intensity mapping survey, which has a small bias, close to 1, and a galaxy survey with larger bias. This suggests a multi-wavelength synergy—a radio and an optical/near-infrared experiment. Since they are planned to deliver data at about the same time, we focus on an HI intensity mapping survey that will be performed with SKA phase 1 in 'single dish mode (Maartens et al. 2015; Santos et al. 2015), together with a Euclid-type galaxy survey (Laureijs et al. 2011; Amendola et al. 2013). We opt for the planned photometric galaxy survey because it will detect a larger number of galaxies than the spectroscopic option. Despite the fact that photo-z measurements are less accurate, the larger statistics ensures a reduced Poisson noise, crucial for optimising MT capabilities. We also consider variations to this survey with different noise and sky coverage, similar to a second-generation galaxy survey such as the Large Synoptic Survey Telescope (hereafter LSST; LSST Dark Energy Science Collaboration 2012; Bacon et al. 2015).

For each tracer and redshift bin, one needs to specify the Gaussian halo bias $b_{\rm G}(z)$, the magnification bias $\mathcal{Q}(z)$, the selection function $n^A(z)$ and the noise angular power spectrum. For a galaxy survey, we define the magnification bias as $\mathcal{Q}^{\rm PG}(z, \mathcal{F}_*) \equiv [-\partial \ln N^{\rm PG} / \partial \ln \mathcal{F}]_{\mathcal{F} = \mathcal{F}_*}$, where $N^{\rm PG}(z, \mathcal{F} > \mathcal{F}_*)$ is the background galaxy number density at redshift z with flux $\mathcal{F}$ above the detection threshold $\mathcal{F}_*$.

HI INTENSITY MAPPING EXPERIMENT (HI). In HI intensity mapping, all galaxies with neutral hydrogen will

contribute to the measured signal. The Gaussian HI bias, $b_G^{HI}(z)$, is computed by weighting the halo bias with the HI content in the dark matter haloes (Santos et al. 2015). The number of observed sources is independent of the flux limit but the temperature perturbation is proportional to Eq. (1) assuming $\mathcal{Q}^{HI} = 1$ (Hall et al. 2013). The selection function follows the HI temperature, viz. $n^{HI}(z) \propto T_{HI}(z)$ (Alonso et al. 2015b), which we fit based on the results of Santos et al. (2015). The noise angular power spectrum in the i-bin of frequency width $\Delta\nu_i$ for an experiment with N_d collecting dishes, total observation time t_{tot} and observed fraction of the sky f_{sky}, is given by

$$\mathcal{N}_{HI}^{ij} = \frac{4\pi f_{sky} T_{sys}^2}{2N_d t_{tot} \Delta\nu_i} \delta^{ij}, \qquad (4)$$

where $T_{sys} = 25 + 60 \times (300\,MHz/\nu)^{2.55}$ K is the system temperature. For SKA1, we assume $N_d \times t_{tot} = 2 \times 10^6$ hr and $f_{sky} = 0.72$.

Note that there is also a shot noise term in intensity mapping, since the signal requires the existence of galaxies in order to produce the emission lines. However, for HI, this shot noise term is quite small and can be safely neglected (Gong et al. 2011).

PHOTOMETRIC GALAXY SURVEY (PG). The bias, magnification bias and selection function that we adopt are (Amendola et al. 2013; Raccanelli et al. 2015)

$$b_G^{PG}(z) = \sqrt{1+z}, \qquad (5)$$
$$\mathcal{Q}^{PG}(z) = 0.2985 + 0.5305z - 0.1678z^2 + 0.2578z^3, \qquad (6)$$
$$n^{PG}(z) \propto z^2 \exp\left[-(1.412z/0.9)^{3/2}\right], \qquad (7)$$

where the proportionality in the last equation is set by the total number of galaxies detected. Figure 1 shows the Gaussian bias of the two tracers as a function of redshift. The fact that the two biases are substantially different enhances the power of the MT. Below we also investigate the effects of increasing the amplitude of the galaxy bias, and consider $b_G^{PG}(z) = 1 + z$.

For a galaxy survey the noise angular power spectrum is dominated by shot-noise, i.e.

$$\mathcal{N}_{PG}^{ij} = \frac{\delta^{ij}}{N_{PG}^i}, \qquad (8)$$

where N_{PG}^i is the number of galaxies per steradian in the ith bin. For the scatter between the photometric redshift estimate and the true redshift, we use $\sigma_{ph}(z) = 0.05(1+z)$ (Ma et al. 2005).

We consider three observational scenarios: (i) a Euclid-like survey detecting 30 galaxies per square arcminute and covering 15,000 square degrees, with 50% overlap with the SKA1 HI experiment; (ii) the same case but with 100% overlap; (iii) a more futuristic LSST-like survey detecting 40 galaxies per square arcminute and covering the whole SKA1 sky. Summarising,

$$f_{sky}^{(i)} = \frac{1}{2}f_{sky}^{(ii)} = \frac{1}{4}f_{sky}^{(iii)} = 7500\,deg^2, \qquad (9)$$

$$N_{PG}^{(i)} = N_{PG}^{(ii)} = \frac{3}{4}N_{PG}^{(iii)} = 30\,arcmin^{-2}. \qquad (10)$$

Note that when we refer to a single tracer, we use its value of f_{sky}, while in the case of MT for (i) and (ii)
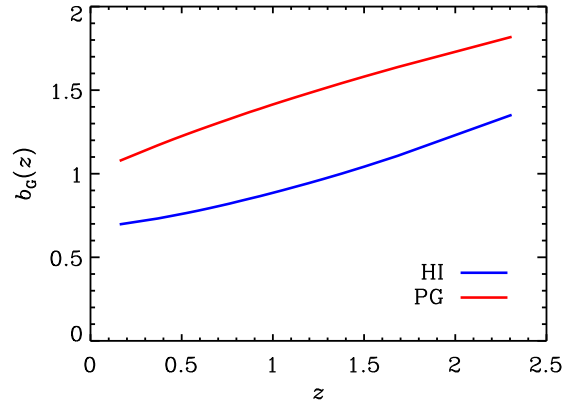

Figure 1. Gaussian bias $b_G(z)$ the 2 surveys.

only the overlapping sky fraction is considered. In other words, the effective sky probed with MT is 0.18, 0.36 and 0.72 for the three photo-z scenarios considered, respectively. Note that for (i) and (ii), we allow the SKA survey to be optimised for the smaller sky area, while maintaining the same total observation time, which will make the noise decrease (Eq. (4)). The same cannot be done for the galaxy survey, since its sky coverage is assumed to be already fixed.

HI-PG CROSS-NOISE. In addition to the noise in the auto-correlations for each tracer, we need to take into account the possible shot-noise cross power spectrum in each bin. This is due to an overlap in the halo mass range which the tracers probe. Even if this is small, it might be important for the MT as this is the only noise showing up in the cross-correlation between tracers. The cross-noise is given by

$$\mathcal{N}_{HI,PG}^{ij} = \frac{\delta^{ij} T_{HI}(z_i)}{\rho_{HI}(z_i) N_{PG}^i} \int dM \frac{dN}{dM} M_{HI}(M)\,\Theta(M), \qquad (11)$$

where dN/dM is the halo mass function, M_{HI} is the mass of neutral hydrogen in a halo of mass M and $\rho_{HI}(z_i)$ is the HI density. If the halo masses probed by the two surveys overlap, then $\Theta(M) = 1$, otherwise it is zero. For further details on the halo mass range for the SKA HI IM survey, see Santos et al. (2015). The mass range for the photo-z survey is found by matching the number of galaxies in the bin given by the halo mass function with the number given by the selection function.

Figure 2 shows the (dimensionless) noise and cross-noise for the chosen binning. The cross-noise is only different from zero at low redshifts, when some haloes will be detected by both surveys. While HI IM is sensitive to the low halo-mass galaxies, galaxy surveys are only sensitive to the most massive haloes. Indeed, for the bins where the cross-noise is different from zero, it is at least two orders of magnitude lower than the cross angular power-spectrum at the large-angle multipoles we are interested in. This might not be the case for more sensitive future surveys (like LSST), which may detect lower mass haloes.

4. FORECASTING METHODOLOGY

We perform a Fisher analysis (Tegmark et al. 1997), working under the assumption that for Gaussian likelihoods the inverse of the Fisher matrix approximates well
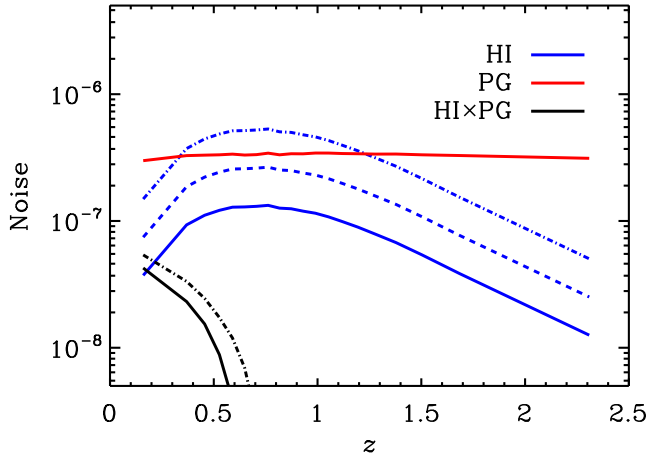
Figure 2. Dimensionless noise and cross-noise. The three HI curves are for $f_{\rm sky} = 0.18$, 0.36 and 0.72 from bottom to top, corresponding to the PG scenarios in Eq. (9). Note that (i) and (ii) have the same cross-noise, since $N_{\rm PG}^{(i)} = N_{\rm PG}^{(ii)}$.

the parameter covariance. The set of parameters is

$$\vartheta_\alpha = \{f_{\rm GR}, f_{\rm NL}, \ln A_s, \ln \Omega_{\rm DM}, \ln b_i^A, \ln \mathcal{Q}_i\}, \qquad (12)$$

with $b_i^A \equiv b_{\rm G}^A(z_i)$ and $\mathcal{Q}_i \equiv \mathcal{Q}^{\rm PG}(z_i)$. We emphasise that we consider a bias parameter for each redshift bin, since due to the high precision measurements we are achieving with the MT technique, using a smaller number of bins with interpolation of parameters might impose a rather strong prior.

We assume a fiducial concordance cosmology with $H_0 = 67.74\,{\rm km/s/Mpc}$, cold dark matter fraction $\Omega_{\rm DM} = 0.26$, baryon fraction $\Omega_b = 0.05$, amplitude of primordial scalar perturbations $A_s = 2.142 \times 10^{-9}$, $f_{\rm GR} = 1$ and $f_{\rm NL} = 0$. The fiducial values for the galaxy bias and magnification bias are set by the survey specifications in § 3. The new parameter $f_{\rm GR}$, used for quantifying how well we will be able to measure GR effects, is defined by

$$C_\ell = C_\ell^{\delta + {\rm RSD} + {\rm lens}} + f_{\rm GR} C_\ell^{\rm GR}, \qquad (13)$$

where $C_\ell^{\delta + {\rm RSD} + {\rm lens}}$ accounts for auto- and cross-correlations between the density, RSD and lensing terms. The term $C_\ell^{\rm GR}$ includes all auto- and cross-correlations of the GR horizon-scale terms. As shown bellow, the reason for this definition of $f_{\rm GR}$ lies in the fact that we can compute $\partial C_\ell / \partial f_{\rm GR}$ fully analytically. We include all effects in Eq. (1) at the same time in order not to bias the accuracy on parameter reconstruction (see e.g. Namikawa et al. 2011; Camera et al. 2015a,b).

We use 20 redshift bins in the range $0 < z < 3$, with variable size such that approximately the same number of photo-z galaxies resides in each bin. Then, we adopt exactly the same redshift binning for SKA1 HI intensity mapping, so that there is a complete overlap between the two tracers. We can do so thanks to the high resolution of an intensity mapping experiment, which allows us to tune the frequency (and so redshift) windows. For the MT covariance matrix, we follow Ferramacho et al. (2014). Note that, since we only concentrate on large scales, we neglect the beam effects due to the angular resolution of the experiments, which should be negligible for small ℓ.

The angular power spectra for MT are computed for

Gaussian window function using a modified version of the publicly available CAMB_sources code (Challinor & Lewis 2011). We changed the code to include options for different selection functions.

We implement numerous improvements in the Fisher matrix analysis in order to ensure its numerical stability. First of all, derivatives with respect to $f_{\rm GR}$ and $\ln b_i^A$ are performed in a fully analytical way. For numerical differentiation with respect to other parameters, we use the five-point stencil method for the four-step derivative. We use the logarithm of the parameter, rather than the parameter itself. This renders the Fisher matrix less prone to numerical issues, as by doing so the gap between the largest and smallest entries of the matrix will be on a logarithmic scale. The marginal error will thus be the relative error with respect to the parameter fiducial value, $\sigma(\ln \vartheta_\alpha) = \sigma(\vartheta_\alpha)/\vartheta_\alpha$.

The high dimensionality of the tomographic matrices (due to the many redshift bins employed) and the large number of nuisance parameters (40 $\ln b_i^A$'s and 20 $\ln \mathcal{Q}_i$'s) require utmost control on the matrix operations. Therefore, we perform matrix inversion via 'inverse diagonalisation': given a square matrix, its inverse is $\mathbf{A}^{-1} = \mathbf{U}\mathbf{\Lambda}^{-1}\mathbf{U}^{-1}$, where $\mathbf{U}$ and $\mathbf{\Lambda}$ are respectively the matrices of the eigenvectors and eigenvalues of $\mathbf{A}$. Thus, $\mathbf{\Lambda}$ is diagonal by construction, and its inversion is trivial. This also helps in removing degeneracies in the Fisher matrix. Indeed, when marginalising over the set of nuisance parameters, if one or more eigenvalues (nearly) vanish, then this degeneracy does not propagate into the cosmological parameters of interest (Camera et al. 2012).

5. DISCUSSION OF RESULTS

Unless otherwise stated, we assume configuration (i) for the photo-z survey, which is the more near-term scenario. For the Fisher matrix, we set the maximum available angular scale, $\ell_{\rm min}$, to 2, and consider two different minimum angular scales, $\ell_{\rm max} = 60$ and 300. Table 1 shows the 1σ marginal error on $f_{\rm GR}$ and $f_{\rm NL}$ for the different tracer configurations, $\ell_{\rm max}$ and nuisance parameters. Given the high dimensionality of both the C_ℓ tomographic matrix and the Fisher matrix, as well as the various implementations ensuring numerical stability of the matrix operations, the computation of the Fisher matrix can become unwieldy as $\ell_{\rm max}$ increases. Therefore in Table 1 we present results for $\ell_{\rm max} = 300$ for the cosmological parameter set, and show the trend due to the inclusion of the nuisance parameters for $\ell_{\rm max} = 60$ only. The big improvement of MT over the single-tracer is apparent: for $f_{\rm NL}$ we get constraints ~ 5 times tighter, and for $f_{\rm GR}$ the improvement is even more impressive, as the bound shrinks by a factor > 20. Moreover, MT is more robust when we allow for full uncertainty on the bias-related nuisance parameters, as can be seen in the impact of a 5% prior on the nuisance parameters.

The use of two different maximum angular multipoles is done not for the sake of a conservative vs optimistic comparison: both $\ell_{\rm max}$'s are well within the linear régime and the inclusion, besides A_s, of $\Omega_{\rm DM}$ and the nuisance parameters ensures that we do not over-estimate the constraining power on $f_{\rm NL}$ or $f_{\rm GR}$, even when pushing to small scales. Instead, we want to understand to what extent smaller scales contribute to the signal of PNG or GR effects, both of which are strongest on ultra-large

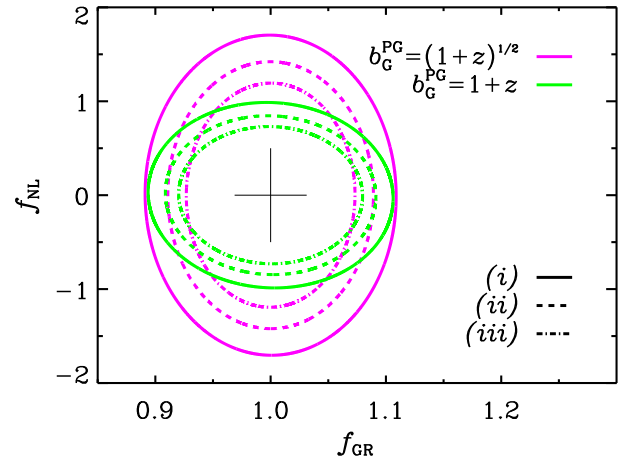| | $\sigma(f_{GR})$ | | | | | | $\sigma(f_{NL})$ | | | | | |
| | HI | | PG | | MT | | HI | | PG | | MT | |
ℓ_{max}	60	300	60	300	60	300	60	300	60	300	60	300
without $\{\ln b_i^A, \ln \mathcal{Q}_i\}$	1.36	1.33	1.58	1.55	0.075	0.072	4.57	4.31	5.34	5.13	1.23	1.12
with $\{\ln b_i^A, \ln \mathcal{Q}_i\}$	1.39	–	1.90	–	0.079	–	5.24	–	6.02	–	1.37	–
with $\{\ln b_i^A, \ln \mathcal{Q}_i\}$ + 5% prior	1.38	–	1.68	–	0.076	–	5.62	–	5.53	–	1.36	–
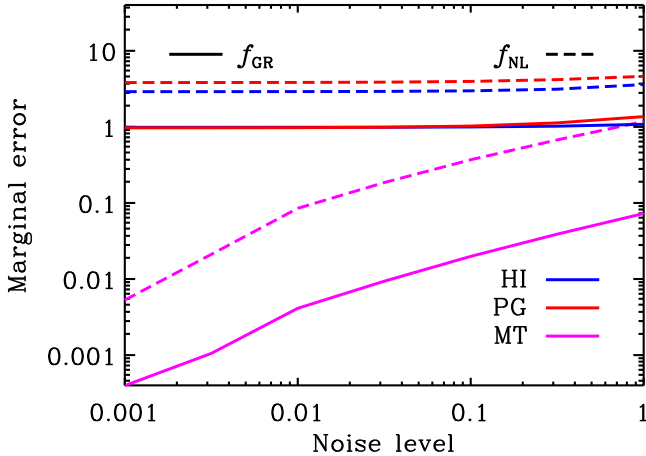
Figure 3. Marginal 1σ error on f_{GR} (solid) and f_{NL} (dashed) versus noise level for SKA1 intensity mapping (blue), Euclid-like photo-z galaxies (red) and MT (magenta) for $\ell_{max} = 100$. As we remove noise, single tracers soon reach the cosmic-variance limited plateau, while MT keeps improving.

Figure 4. Joint 1σ marginal error contours for $\ell_{max} = 300$ without $\{\ln b_i^A, \ln \mathcal{Q}_i\}$ for the two photo-z Gaussian bias models and the three survey scenarios.

Table 2
Marginal errors from the MT analysis for the three photo-z scenarios with Gaussian bias $\sqrt{1+z}$ (or $1+z$) and $\ell_{max} = 300$.

	$\sigma(f_{GR})$		$\sigma(f_{NL})$	
(i)	0.071	(0.070)	1.12	(0.65)
(ii)	0.059	(0.060)	0.94	(0.56)
(iii)	0.048	(0.053)	0.79	(0.48)

scales. Moreover, this also enables us to monitor the impact of noise. Noise usually dominates on small scales and is negligible in the cosmic-variance limited régime, but Ferramacho et al. (2014) suggested that the more MT is effective in 'removing' cosmic variance, the larger the scales at which noise starts becoming relevant.

In Fig. 3 we show the forecast marginal errors on f_{GR} (solid) and f_{NL} (dashed) as a function of the noise level. We multiply the noise of both intensity mapping and galaxy number counts by a fudge factor and let it vary from 0 to 1, where 0 means a noiseless experiment and 1 is the real setting. Even when noise is almost negligible, single tracers reach a cosmic-variance limited plateau, whereas MT constraining power keeps improving. Note that this noise reduction is more important for the galaxy survey as the signal-to-noise for the HI survey is already quite low. The lesson to be learnt is that the more cosmic variance fades, the more important the signal-to-noise ratio becomes.

Seljak et al. (2009) propose a mass-dependent weighting of the detected sources, which can considerably suppress the stochasticity between haloes and dark matter, thus reducing the shot noise contribution. By doing so, they showed that it will be possible for a next-generation Euclid-like survey to reduce the Poisson noise even by 30%. From Fig. 3, the resulting improvement appears crystal clear (see also Hamaus et al. 2011).

Now we want to investigate the impact of f_{sky} and the assumed Gaussian bias b_G^{PG}. First, we perform the same analysis as before, but comparing the three photo-z scenarios (i), (ii) and (iii) described in § 3. Secondly, we swap from the Euclid-like bias of Eq. (5) to

the higher bias $b_G^{PG} = 1 + z$. In Fig. 4 we present the corresponding forecast joint 1σ marginal error contours in the (f_{GR}, f_{NL}) plane. The collapse from the outermost to the middle ellipses is simply caused by the doubling of the surveyed sky areas, but the innermost contours are also affected by a reduced photometric galaxy shot noise, as the number density grows by 30%. Also, we remind the reader that the HI intensity mapping noise is linearly dependent on f_{sky}. Summarising, in Table 2 we quote the forecast marginal errors on the measurement of GR effects and PNG for the three photo-z scenarios and two biases. Results are shown for $\ell_{max} = 300$ and no nuisance parameters.

The MT technique will allow synergies between SKA and Euclid to provide game-changing measurements on horizon scales. We have shown it will be able to probe the inflation régime when $f_{NL} \sim 1$ and make the first ever detections of the GR effects. Moreover, our analysis shows that with this new method, we need to rethink the way large-scale surveys are being designed. Ultra-large volumes are no longer the ultimate goal, as we can cancel cosmic variance when probing these features. Instead, we only need to probe up to the required scale, and maximisation of the signal to noise should be the priority

instead. A survey of about 10,000 deg^2 should be enough for most purposes. This at the same time will make it easier for the SKA1 cosmology survey to be commensal with other science cases. Finally, although we have not addressed specifically the issue of foreground contamination, it is expected that the MT technique will alleviate this problem even further since any possible residuals from the cleaning process (Alonso et al. 2015) and even systematics should be uncorrelated between HI intensity mapping and the photo-z galaxy survey.

REFERENCES

Abramo L. R., Leonard K. E., 2013, Mon. Not. Roy. Astron. Soc., 432, 318

Alonso D., Bull P., Ferreira P. G., Maartens R., Santos M. G., 2015b, arXiv:1505.07596

Alonso D., Bull P., Ferreira P. G., Santos M. G., 2015, Mon. Not. Roy. Astron. Soc., 447, 400

Alonso D., Ferreira P. G., 2015, arXiv:1507.03550

Amendola L., et al., 2013, Living Rev. Rel., 16, 6

Bacon D., Bridle S., Abdalla F. B., Brown M., Bull P., et al., 2015, PoS, AASKA14, 145

Bonvin C., Durrer R., 2011, Phys. Rev., D84, 063505

Camera S., Carbone C., Fedeli C., Moscardini L., 2015a, Phys. Rev., D91, 043533

Camera S., Maartens R., Santos M. G., 2015b, Mon. Not. Roy. Astron. Soc., 451, L80

Camera S., Raccanelli A., Bull P., Bertacca D., Chen X., et al., 2015, PoS, AASKA14, 025

Camera S., Santos M. G., Bacon D. J., Jarvis M. J., McAlpine K., Norris R. P., Raccanelli A., Rottgering H., 2012, Mon. Not. Roy. Astron. Soc, 427

Camera S., Santos M. G., Ferreira P. G., Ferramacho L., 2013, Phys. Rev. Lett., 111, 171302

Camera S., Santos M. G., Maartens R., 2015c, Mon. Not. Roy. Astron. Soc., 448, 1035

Challinor A., Lewis A., 2011, Phys. Rev., D84, 043516

Dalal N., Dore O., Huterer D., Shirokov A., 2008, Phys. Rev., D77, 123514

Ferramacho L. D., Santos M. G., Jarvis M. J., Camera S., 2014, Mon. Not. Roy. Astron. Soc., 442, 2511

Giannantonio T., Porciani C., Carron J., Amara A., Pillepich A., 2012, Mon. Not. Roy. Astron. Soc., 422, 2854

Gong Y., Chen X., Silva M., Cooray A., Santos M. G., 2011, Astrphys. J., 740, L20

Hall A., Bonvin C., Challinor A., 2013, Phys. Rev., D87, 064026

Hamaus N., Seljak U., Desjacques V., 2011, Phys. Rev., D84, 083509

Laureijs R., et al., 2011, ESA-SRE, 12

LSST Dark Energy Science Collaboration, 2012, arXiv:1211.0310

Ma Z.-M., Hu W., Huterer D., 2005, Astrophys. J., 636, 21

Maartens R., Abdalla F. B., Jarvis M., Santos M. G., 2015, PoS, AASKA14, 016

Matarrese S., Verde L., 2008, Astrophys. J., 677, L77

McDonald P., Seljak U., 2009, JCAP, 0910, 007

Montanari F., Durrer R., 2015, arXiv:1506.01369

Namikawa T., Okamura T., Taruya A., 2011, Phys. Rev., D83, 123514

Planck Collaboration, Ade P. A. R., Aghanim N., Arnaud M., Arroja F., Ashdown M., Aumont J., Baccigalupi C., Ballardini M., Banday A. J., et al., 2015, arXiv:1502.01592

Raccanelli A., Montanari F., Bertacca D., Doré O., Durrer R., 2015, arXiv:1505.06179

Santos M., Bull P., Alonso D., Camera S., Ferreira P., et al., 2015, PoS, AASKA14, 019

Seljak U., 2009, Phys. Rev. Lett., 102, 021302

Seljak U., Hamaus N., Desjacques V., 2009, Phys. Rev. Lett., 103, 091303

Tegmark M., Taylor A., Heavens A., 1997, Astrophys. J., 480, 22

Yamauchi D., Takahashi K., Oguri M., 2014, Phys. Rev., D90, 083520

Yoo J., 2010, Phys. Rev., D82, 083508

Yoo J., Hamaus N., Seljak U., Zaldarriaga M., 2012, Phys. Rev., D86, 063514